

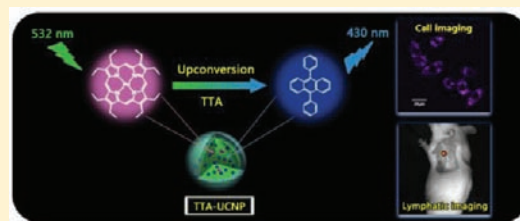
Blue-Emissive Upconversion Nanoparticles for Low-Power-Excited Bioimaging in Vivo

Qian Liu, Tianshe Yang, Wei Feng, and Fuyou Li*

Department of Chemistry and State Key Laboratory of Molecular Engineering of Polymers and Institute of Biomedicine Science, Fudan University, Shanghai 200433, People's Republic of China

S Supporting Information

ABSTRACT: Water-soluble upconversion luminescent (UCL) nanoparticles based on triplet–triplet annihilation (TTA) were successfully prepared by co-loading sensitizer (octaethylporphyrin Pd complex) and annihilator (9,10-diphenylanthracene) into silica nanoparticles. The upconversion luminescence quantum yield of the nanoparticles can be as high as 4.5% in aqueous solution. As determined by continuous kinetic scan, the nanoparticles have excellent photostability. Such TTA-based upconversion nanoparticles show low cytotoxicity and were successfully used to label living cells with very high signal-to-noise ratio. UCL imaging with the nanoparticles as probe is capable of completely eliminating background fluorescence from either endogenous fluorophores of biological sample or the colabeled fluorescent probe. In particular, such blue-emissive upconversion nanoparticles were successfully applied in lymph node imaging in vivo of living mouse with excellent signal-to-noise ratio (>25), upon low-power density excitation of continuous-wave 532 laser (8.5 mW cm^{-2}). Such high-contrast and low-power excited bioimaging in vivo with a blue-emissive upconversion nanoparticle as probe may extend the arsenal of currently available luminescent bioimaging in vitro and in vivo.



INTRODUCTION

Upconversion luminescence (UCL) is a unique process where continuous-wave (CW) low-energy photons are converted into high-energy ones.^{1,2} Rare-earth-based materials codoped with Yb^{3+} and Er^{3+} (or Tm^{3+}) show excellent upconversion luminescence under CW excitation of 980 nm,³ which is distinguished from two-photon fluorescence with pulse excitation of extremely high power density ($\sim 10^6 \text{ W cm}^{-2}$).⁴ Rare-earth-based upconversion nanophosphors (RE-UCNPs) have successfully been achieved as luminescence probes for whole-body imaging of small-animals,^{5–8} showing the absence of autofluorescence from biological samples.^{6a,b} However, RE-UCNPs suffer from two fundamental drawbacks, that is, low absorption cross-section of the Yb^{3+} sensitizer ($\sim 10^{-20} \text{ cm}^2$)⁹ and quite low UCL quantum yield (ϕ_{UCL}).^{7,10} For example, the reported ϕ_{UCL} of sub-10 nm $\text{NaLuF}_4:\text{Yb},\text{Tm}$ nanocrystals in powder form is only $\sim 0.47\%$.⁷ As a result, a relatively high power density ($10^2\text{--}10^3 \text{ mW cm}^{-2}$) from a 980 nm laser is required for whole-body small-animal imaging,^{5–8} leading to the presence of overheating effect.⁸

Recently, triplet–triplet annihilation (TTA)-based upconversion luminescence (TTA-UCL) has emerged as another efficient process with anti-Stokes shift upon excitation by low-power laser ($\sim \text{mW cm}^{-2}$).^{2,11–14} The sensitized TTA mechanism involves the transfer of energy between a sensitizer molecule and an annihilator.¹⁴ As compared to the rare-earth-based UCL process, TTA-UCL has some advantages including intense absorption coefficient of sensitizer ($\sim 10^{-17} \text{ cm}^2$) and high quantum yield.² For example, Castellano and co-workers

have reported that the solution of a BODIPY dye (annihilator) and Pt-tetraphenyltetraabenzoporphyrin (sensitizer) in benzene shows a TTA-based ϕ_{UCL} of 15.1%.^{12a} Unlike the fixed excitation and emission wavelengths of RE-UCNPs, moreover, TTA-UCL-based systems show tunable excitation and emission wavelengths by judicious selection of the sensitizer and the acceptor independently. The excitation and emission wavelengths can be tuned in the regions of 410–780 and 360–560 nm, respectively.^{2,11–14} To date, a series of TTA-based upconversion systems have successfully been developed.

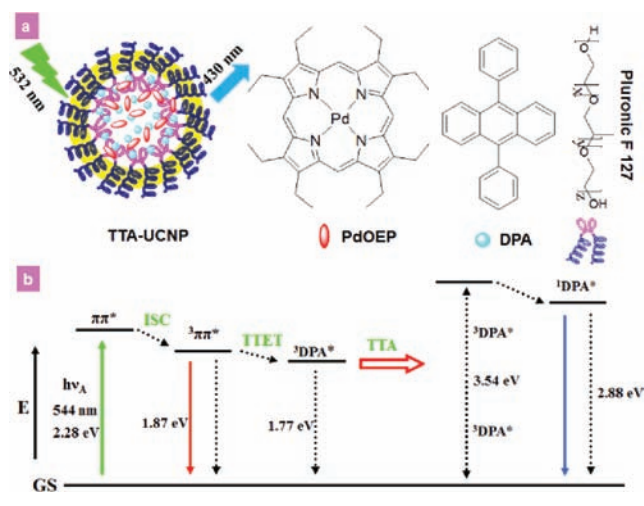
However, most of the reported TTA-based upconversion systems have been fabricated in organic solution (such as toluene, chloroform, benzene, and dichloromethane),^{2,11–14} which limits their application in bioimaging. Recently, some effective TTA-supported upconversion emitters could be achieved in the polymer films such as ethyleneoxide–epichlorohydrin copolymer (EO–EPI) and the polyurethanes.^{12c,d} Nowadays, few TTA-based upconversion systems have been reported to be water-soluble.¹⁵ In particular, no TTA-based upconversion material has been used for whole-body imaging in vivo of small animal.

In the present study, we have developed a strategy of embedding both sensitizer and annihilator into one silica nanoparticle (Scheme 1a) to fabricate a water-soluble TTA-based upconversion nanoparticle (named TTA-UCNP). This nanoparticle shows blue upconversion luminescence ($\lambda_{\text{em}} = 433 \text{ nm}$) with high ϕ_{UCL} of 4.5% in pure water. Importantly,

Received: January 12, 2012

Published: February 27, 2012

Scheme 1. (a) Schematic Illustration of Upconversion Luminescence of the Nanoparticles TTA-UCNP, and Chemical Structures of PdOEP, DPA, and F127; and (b) Energy Level Diagram Describing the Sensitized Triplet–Triplet Annihilation Process between PdOEP and DPA in the TTA-UCNP^{12d}



such blue-emissive nanoparticle was successfully used for upconversion luminescence imaging of lymph node *in vivo* of whole-body small animal under low power density excitation at 532 nm (8.5 mW cm^{-2}).

EXPERIMENTAL SECTION

Materials. All reagents and solvents were used as received without further purification. Nonionic surfactant Pluronic F127, tetraethyl orthosilicate (TEOS, 99.99%), diethoxydimethylsilane (DEDMS, 97%), Pd complex octaethylporphyrin (PdOEP), 9,10-diphenylanthracene (DPA), rhodamine B, phosphate buffered saline (PBS), fetal bovine serum (FBS), and methyl thiazolyl tetrazolium were purchased from Aldrich. Hoechst 33258 and cell culture reagents were purchased from Invitrogen. Reagent grade toluene and hydrochloric acid (fuming, $\geq 37\%$) were purchased from Sinopharm Chemical Reagent Co., Ltd. Deionized water was used in the experiments throughout.

Synthesis of Silica Nanoparticles Loaded with PdOEP and DPA (TTA-UCNP). The nanoparticles TTA-UCNP were synthesized according to a previously reported procedure¹⁶ with suitable modification. In a 20 mL glass scintillation vial, 2.0 g of Pluronic F127, 1.0 mg ($1.56 \times 10^{-6} \text{ mol}$) of PdOEP, and 10 mg ($3.03 \times 10^{-5} \text{ mol}$) DPA were carefully soluble in toluene. The solvent was evaporated from the homogeneous lavender organic solution by means of a gently nitrogen flow and subsequently under vacuum. The solid residue was then dissolved under magnetic stirring with 100 mL of HCl (0.85 mol L^{-1}). TEOS (2 mL) was then added to the resulting aqueous solution followed by DEDMS (450 μL , 2.1 mmol) after 6 h. The mixture was kept under stirring for 48 h at 25 °C before dialysis/ultrafiltration treatments and measurements.

Characterization. The size and morphology of the TTA-UCNP were determined at a JEOL JEM-2010 transmission electron microscope operated at 200 kV. These as-prepared samples were dispersed in H₂O and dropped on the surface of a copper grid for TEM test. Before dynamic light scattering (DLS) measurements, the sample was filtered through 0.8 μm Millipore filters (hydrophilic Millex-LCR, mixed cellulose ester) to remove dust. The measurement was performed with a fixed scattering angle of 90°. The sample was measured by an ALV-5000 laser light scattering spectrometer. X-ray photoelectron spectroscopy analysis (XPS) experiments were carried out on a RBD upgraded PHI-5000C ESCA system (Perkin-Elmer) with Mg K α radiation ($h\nu = 1253.6 \text{ eV}$) or Al K α radiation ($h\nu = 1486.6 \text{ eV}$). The upconversion luminescence emission spectra were recorded on an Edinburgh LFS-920 instrument, but the excitation

source used an external 0–500 mW adjustable 532 nm semiconductor laser (Changchun fs-optics Co., China) with an optic fiber accessory, instead of the xenon source in the spectrophotometer. The photos of upconversion luminescence emission were obtained digitally on a Nikon multiple CCD Camera. UV–vis absorption spectra were recorded on a Shimadzu 3000 spectrophotometer.

Measurement of Upconversion Luminescence Quantum Yield. The upconversion luminescence quantum yield (ϕ_{UCL}) of the TTA-UCNP in water was determined according to eq 1,¹⁷ with rhodamine B in ethanol as a standard reference. The equation is multiplied by a factor of 2 to make the maximum quantum yield to be unity.

$$\Phi_{\text{UCL}} = 2\Phi_{\text{std}} \left(\frac{A_{\text{std}}}{A} \right) \left(\frac{I_{\text{UCL}}}{I_{\text{std}}} \right) \left(\frac{\eta}{\eta_{\text{std}}} \right)^2 \quad (1)$$

where ϕ_{UCL} and ϕ_{std} stand for upconversion luminescence quantum yield of sample TTA-UCNP and fluorescence quantum yield of rhodamine B, respectively. A and A_{std} stand for absorbances of the TTA-UCNP and rhodamine B, respectively. I_{UCL} and I_{std} stand for integrated upconversion luminescence intensity of the TTA-UCNP and fluorescence intensity of rhodamine B, respectively. η and η_{std} stand for the refractive index of water (for the TTA-UCNP) and ethanol (for rhodamine B), respectively.

Cell Culture. The HeLa lines were provided by the Institute of Biochemistry and Cell Biology, SIBS, CAS (China). The HeLa cells were grown in DMEM (Dulbecco's modified Eagle's medium) supplemented with 10% FBS (fetal bovine serum). The cell culture was at 37 °C under 5% CO₂.

Cytotoxicity Assay. The *in vitro* cytotoxicity was measured using a standard methyl thiazolyl tetrazolium (MTT, Sigma-Aldrich) assay in HeLa cell lines. Briefly, cells growing in log phase were seeded into a 96-well cell-culture plate at 1×10^4 /well. The nanoparticles TTA-UCNP (100 μL /well) at a concentration of 20, 40, 80, 160, or 320 $\mu\text{g}/\text{mL}$ was added to the wells of the treatment group, using 100 μL /well DMEM as the negative control group. The cells were incubated at 37 °C under 5% CO₂ for 5 or 24 h, respectively. The combined MTT/PBS solution was added to each well of the 96-well assay plate and was incubated for an additional 3 h. An enzyme-linked immunosorbent assay (ELISA) reader (infinite M200, Tecan, Austria) was used to measure the OD570 (absorbance value) of each well referenced at 690 nm. The following formula was used to calculate the viability of cell growth: viability (%) = (mean of absorbance value of treatment group/mean absorbance value of control) $\times 100$.

Cellular Staining. To ensure complete dispersion of the TTA-UCNP in PBS, the solution ($40 \mu\text{g mL}^{-1}$) was obtained from an ultrasonic to get homogeneous colloidal solution. HeLa cells were stained with $40 \mu\text{g mL}^{-1}$ TTA-UCNP in a 5% CO₂ incubator at 37 °C for 3 h; cell imaging was then carried out after washing the cells with PBS three times to remove the excess TTA-UCNP.

Confocal Upconversion Luminescence Microscopy Imaging of Living Cells Incubated with TTA-UCNP. Confocal upconversion luminescence microscopy imaging of living HeLa cells incubated with the TTA-UCNP was performed on our modified microscope. The instrument was built on an inverted microscope (Olympus IX81, Japan) and a confocal scanning unit (FV1000, Olympus, Japan). For the upconversion luminescence microscopy imaging, the continuous-wave (CW) laser at 543 nm provided the excitation, and upconversion luminescence emission at 420–480 nm was collected as output signal. In addition, the reverse excitation dichroic mirror (excitation DM, short-pass, edge at 500 nm, model 500DMSP, OMEGA) was adopted. A photomultiplier tube (R6357 enhanced model, HAMAMATSU, Japan) was used as a detector. For confocal fluorescence microscopy imaging, the CW laser at 405 nm provided the excitation, and fluorescence emission was collected at 420–480 nm. A 60 \times oil-immersion objective lens was used.

In Vivo and ex Vivo Upconversion Luminescence Imaging of Lymphatic Node of Kunming Mouse. To perform upconversion luminescence lymphatic imaging, the upconversion luminescence *in vivo* imaging system was built. Two external 0–500 mW adjustable

532 nm semiconductor lasers were used as the excitation source, and a cooled electron-multiplying charge-coupled device (EMCCD, Andor DU897) was used as the signal collector. First, 20 μL of TTA-UCNP was injected intradermally into the claw. At 30 min postinjection, upconversion luminescence lymphatic imaging in vivo was performed under excitation at 532 nm (the power density of 8.5 mW cm^{-2}) when emission at $<525 \text{ nm}$ was collected with short-pass filter (transmission at 532 nm of $<1 \times 10^{-6}$). For ex vivo imaging, lymph node was harvested from mouse injected with the TTA-UCNP for 30 min.

Histology Study. Tissue samples were harvested from mice injected with the TTA-UCNP 30 min postinjection. The lymph node was fixed in pentanediol, embedded in paraffin, sectioned, and stained with hematoxylin and eosin. The histological sections were observed under an optical microscope.

RESULTS AND DISCUSSION

Commonly, blue fluorescence material is unsuitable for small-animal imaging, because of serious autofluorescence from biological samples upon UV excitation. Herein, in our design strategy, a blue-emitting upconversion system (Scheme 1b) with an annihilator of 9,10-diphenylanthracene (DPA, $\lambda_{\text{em}} = 433 \text{ nm}$) and a sensitizer of octaethylporphyrin Pd complex (PdOEP)^{12c,d,h} was deliberately adopted to investigate if blue-emissive upconversion material can be used for small-animal imaging. PdOEP has a high absorption cross-section of $8.5 \times 10^{-17} \text{ cm}^2$ at 546 nm, and such a system of DPA and PdOEP has been successfully fabricated into an effective TTA-supported upconversion emitter in an organic phase and a polymer film by Castellano and co-workers.^{12c,d,h} Scheme 1b shows the energy level diagram of the sensitized triplet–triplet annihilation process between PdOEP and DPA.

Nanoparticle Characterization. In light of the relative low cytotoxicity and high stability of silica-based materials, herein, SiO_2 nanoparticles have been used for fabricating TTA-UCL emitter. A direct micelle assisted method was employed to fabricate nanoparticles (TTA-UCNP), using polyethyleneglycol F127 to load sensitizer PdOEP and annihilator DPA into silica layer.¹⁶ The as-prepared SiO_2 nanoparticle loaded with PdOEP and DPA is abbreviated as TTA-UCNP and was characterized by transmission electron microscopy (TEM), dynamic light scattering (DLS), and X-ray photoelectron spectroscopy (XPS) analysis.

As shown in Figure 1a, the TEM image indicated that the TTA-UCNP consists of uniform spherical nanoparticles with a diameter of roughly $10 \pm 1.6 \text{ nm}$. As measured by DLS

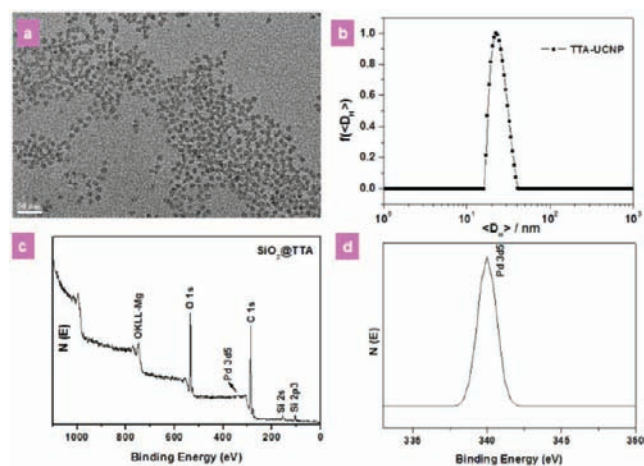


Figure 1. Transmission electron microscopy (a), dynamic light scattering (b), and X-ray photoelectron spectroscopy (c) and (d, palladium) of the TTA-UCNP.

technique, the hydrodynamic diameter of the TTA-UCNP is $22.5 \pm 6.9 \text{ nm}$ (Figure 1b). The hydrodynamic diameter is larger than the diameter measured by TEM, suggesting that the PEG chains of F127 in the TTA-UCNP are extended in the aqueous solution.¹⁶

The successful loading of PdOEP and DPA into silica nanoparticles was confirmed by X-ray photoelectron spectroscopy (XPS) and standard absorption curve analysis. XPS measurement confirmed the existence of the elements Si and Pd (Figure 1c and d). In the absorption spectrum of TTA-UCNP (Figure 2), the appearance of the characteristic bands of

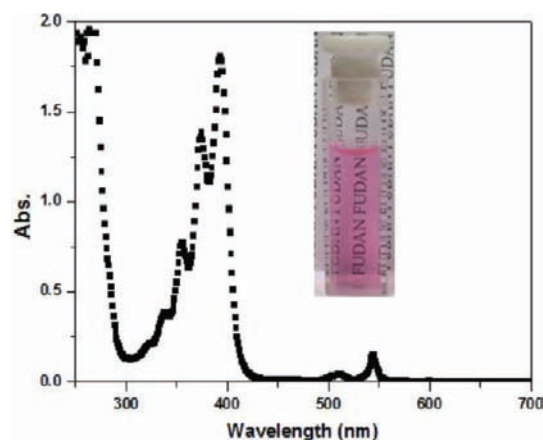


Figure 2. Absorption spectrum of the TTA-UCNP dispersed in water. Inset: Bright-field photo of the TTA-UCNP dispersed in water inside the 1 cm cuvette.

PdOEP (at 546 and 515 nm) and DPA (at 375 and 356 nm) indicates the coexistence of PdOEP and DPA in the TTA-UCNP. Furthermore, as determined by standard absorption spectroscopy, the molar ratio of PdOEP to DPA, which were loaded in silica nanoparticles, is 1:14 (Figure S2). The loading proportions of PdOEP and DPA in the TTA-UCNP can be calculated to be 72 and 54 mol %, respectively.

Upconversion Luminescence Properties of TTA-UCNP. Selective excitation of the TTA-UCNP system ($\lambda_{\text{ex}} = 532 \text{ nm}$) generates the upconversion luminescence (UCL) emission peaked at 433 nm, which is matched with the fluorescence wavelength of DPA excited with 375 nm (Figures 3a and S3). The blue upconversion luminescence is visible to the naked eye, as shown in Figure 3a, inset. The integrated UCL intensity of TTA-UCNP was enhanced as the incident laser power increased (Figure 3b). As shown in Figure 3c, the UCL intensity is proportional to the square of the incident laser power over the range of 0–360 mW cm^{-2} . The solid line in Figure 3c shows the best quadratic fit (χ^2) to the data, confirming the nature of the nonlinear photochemistry. With rhodamine B as a reference,¹⁷ the upconversion luminescence quantum yield (Φ_{UCL}) of the TTA-UCNP in pure water was measured to be 4.5% (260 mW cm^{-2}), which is the highest reported value of Φ_{UCL} for water-soluble upconversion materials (including rare-earth upconversion nanophosphors) so far.

Moreover, the possible photobleaching of the TTA-UCNP system was considered. No significant change in the UCL emission was observed when the TTA-UCNP was continuously irradiated by the CW 532 nm laser (360 mW cm^{-2}) for more than 30 min (Figure S4), suggesting excellent photostability for TTA-UCNP.

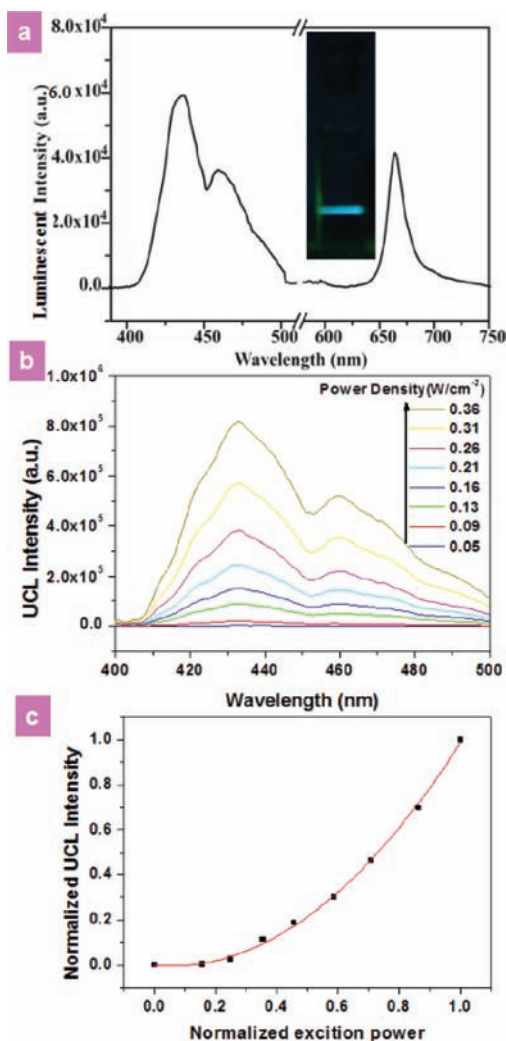


Figure 3. (a) Luminescence emission spectrum and emission photo (inset, with short-pass filter at 532 nm) of the TTA-UCNP dispersed in water inside the 1 cm cuvette ($\lambda_{\text{ex}} = 532$ nm). (b) Upconversion luminescence intensity profile of the TTA-UCNP as a function of 532 nm incident power. (c) Normalized integrated emission intensity data from part (b) plotted as a function of incident power. The solid red line is the best quadratic fit (χ^2) to the emission data, normalized to the highest incident intensity (360 mW cm^{-2}).

Cytotoxicity of TTA-UCNP. The long-term cellular toxicity of the TTA-UCNP toward the HeLa cell lines was determined by means of an MTT assay. In the presence of a TTA-UCNP concentration of $<320 \mu\text{g mL}^{-1}$, the cellular viabilities were estimated to be greater than 90% after incubation for 24 h (Figure 4). The results indicate that the TTA-UCNP is generally low toxic on cell proliferation. In particular, in the luminescence cellular imaging (conditions: incubation time of 3 h, TTA-UCNP concentration of $40 \mu\text{g mL}^{-1}$), no inhibition on cell proliferation was observed, as shown in Figure 4.

Confocal Upconversion Luminescence Imaging of Living Cell. The schematic layout of a confocal upconversion luminescence microscopy (CUCLM) system setup was shown in Figure 5a. The excitation beam path from continuous-wave (CW) laser at 543 nm is shown in green, and the upconversion emission pathway (at 420–480 nm) is shown in blue. Herein, the excitation and emission lights could be separated by a reverse excitation dichroic mirror. The excited CW laser at

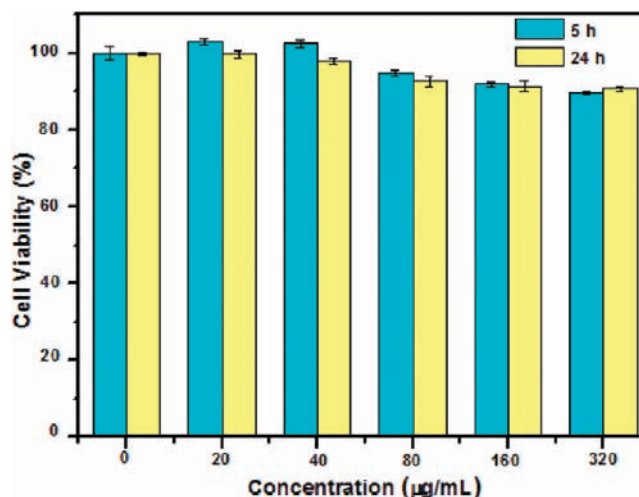


Figure 4. In vitro cell viability of HeLa cells incubated with TTA-UCNP at different concentrations for 5 and 24 h.

543 nm was directed by the galvanometer mirrors and then focused by an objective lens into the specimen. Upconversion luminescence light emitted from the scanning spot was deflected by the galvanometer mirrors and then passed through the reverse dichroic mirror, a confocal pinhole, and a filter, and finally entered a photomultiplier tube (detector).

Further application of TTA-UCNP in bioimaging was demonstrated using this confocal upconversion luminescence microscopy (CUCLM). When the HeLa cells were incubated with the TTA-UCNP at 37°C for 3 h, upconversion luminescence (UCL) signals at 420–480 nm were detected upon excitation at CW 543 nm (Figure 5b). Further Z-scan imaging confirms that the TTA-UCNP was internalized into the cells (Figure S7). Moreover, when excited with 405 nm light, conventional fluorescence signals at 420–480 nm from the annihilator DPA were detected (Figure 5c) and were merged with intracellular UCL signals perfectly (Figure 5d), indicating that the intracellular UCL signal at 420–480 nm is originated from DPA in the TTA-UCNP.

Moreover, quantization of the UCL profile across the line shown in the inset of Figure 5e reveals an excellent signal-to-noise ratio (SNR), with extremely high UCL signals (counts >1500 for region 2 and region 4) and no background luminescence (counts ~ 0 for region 1 and region 3) (Figure 5e). Such high UCL SNR indicated that biosamples have very low probability of UCL emission under CW excitation at 543 nm. Moreover, as compared to the normal fluorescence imaging with 405 nm excitation, TTA-UCL imaging provides lower photobleaching. For example, after 600 s illumination by a 543 nm laser with a higher power (0.57 mW), the UCL signal from intracellular TTA-UCNP still retained 99% of its initial intensities (Figure 5f), whereas the fluorescence signal of DPA decreased rapidly to 1% of its initial value in a control experiment with lower power of 405 nm illumination (0.15 mW).

Furthermore, TTA-UCNP and commercial nuclear-stain Hoechst 33258 were used to colabel the living HeLa cell (Figures 6 and S8). When excited at 405 nm, intense fluorescent signals in the nucleus (from Hoechst 33258) were observed (Figure 6a and c). In contrast, no signal from the nucleus was detected in the UCL image of a cell ($\lambda_{\text{ex}} = 543$ nm, Figure 6b and c), although the UCL detection channel (420–480 nm) was deliberately chosen to overlap the fluorescence signal of Hoechst ($\lambda_{\text{em}} = 461$ nm). Thus,

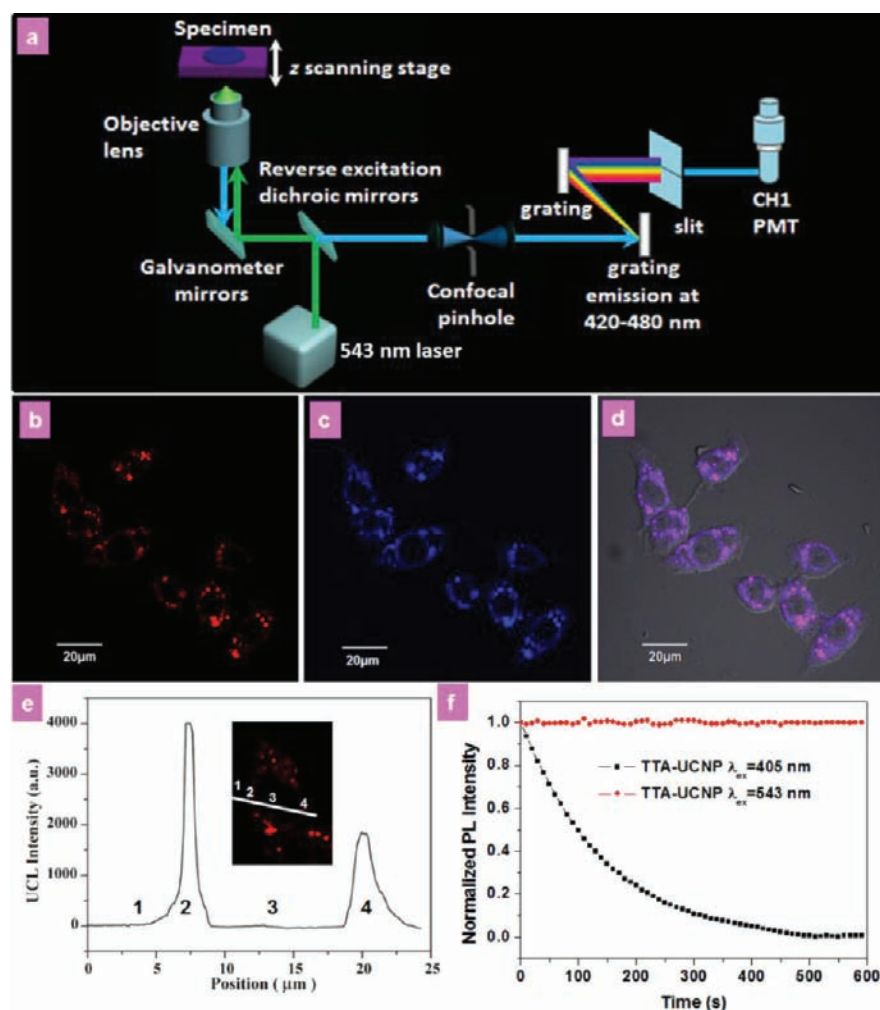


Figure 5. (a) Schematic layout of a confocal upconversion luminescence microscopy system setup. The excitation laser beam path and emission pathway are shown in green and blue, respectively. (b,c) Upconversion luminescence image (b, $\lambda_{\text{ex}} = 543$ nm) and conventional fluorescence image (c, $\lambda_{\text{ex}} = 405$ nm) of living HeLa cell incubated with TTA-UCNP when excited with 543 and 405 nm, respectively. Emission was collected at 420–480 nm. (d) The overlay of bright-field image and panels b and c. (e) Upconversion luminescence intensity along the line shown in the inset. (f) Quantitative analysis of the changes in intracellular luminescence intensities of TTA-UCNP-labeled cells under excitation at 405 or 543 nm. The excitation powers in the focal plane at 405 and 543 nm are ~ 0.15 and ~ 0.57 mW, respectively.

TTA-UCL imaging with the TTA-UCNP as probe is capable of completely eliminating background fluorescence from either endogenous fluorophores or the colabeled fluorescent probe.

In Vivo and ex Vivo UCL Imaging of Lymphatic Node.

The lymphatic system is increasing interrelated with pandemic diseases. Herein, TTA-UCNP was further applied in luminescence lymphatic imaging. Figure 7a shows the schematic layout of the experimental setup for the triplet-triplet annihilation-based upconversion luminescence (TTA-UCL) imaging in vivo system. In this imaging system, two external 0–500 mW adjustable continuous-wave (CW) 532 nm lasers passed the optical fiber into the light-tight box and then passed through beam expanders to be converted into large bundles of beams, which then homogeneously illuminated the whole-body mouse. Upconversion luminescence emission at < 525 nm from the sample passed through a short-pass filter and lens and finally was collected with an EMCCD camera. The excitation beam path from CW laser at 532 nm is shown in green, and the upconversion emission pathway (at < 525 nm) is shown in blue.

Real-time UCL imaging of lymph node in vivo of Kunming mice was performed on this in vivo imaging system, when the TTA-UCNP was injected intradermally into the claw. Upon low-power density excitation of CW 532 nm laser (8.5 mW cm^{-2}), a clear TTA-based UCL signal ($\lambda_{\text{em}} < 525$ nm) was detected in the lymphatic drainage basins of the oxtar (Figure 7b). The imaging ex vivo then confirms the UCL signal from the lymphatic node of the oxtar (Figure 7b). H&E-stained section of lymph node further supported the existence of the TTA-UCNP in lymph node (Figure 8). Figure 8c shows the overlay of UCL image and bright-field image. The significant UCL signal could be observed in H&E-stained sections of lymph node, with extremely high UCL signals (counts > 4095 for regions signal, Figure 8d).

In particular, analysis of the UCL signal in region of interest revealed a high signal-to-noise ratio (SNR of 25, Figure 7b) between the TTA-UCNP and the background (including autofluorescence from biosample and excitation light), although the blue upconversion luminescence was chosen as detection channel. Such TTA-UCL imaging with both high-contrast and low excited power density

of whole-body small animal cannot be achieved for the reported rare-earth upconversion nanophosphors as probe, which contributed to the high absorption cross-section

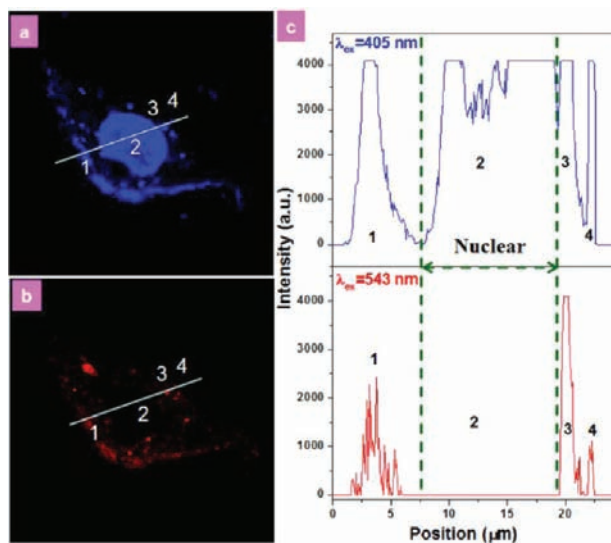


Figure 6. Fluorescence image (a, $\lambda_{\text{ex}} = 405 \text{ nm}$) and upconversion luminescence image (b, $\lambda_{\text{ex}} = 543 \text{ nm}$) of living HeLa cell colabeled with the TTA-UCNP and Hoechst 33258, while the emission was collected at 420–480 nm. Panel c shows the luminescence intensity profile along the lines shown in panel a (top) and panel b (bottom).

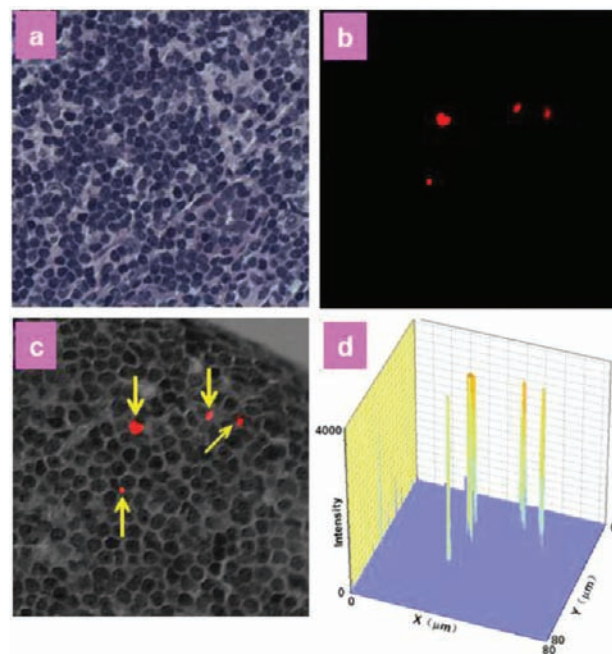


Figure 8. (a) H&E-stained section of lymph node from mice injected with the TTA-UCNP for 30 min. (b,c) Confocal upconversion luminescence microscopy image (b) and its overlay with bright-field image (c) of lymph node ($\lambda_{\text{ex}} = 543 \text{ nm}$, $\lambda_{\text{em}} = 420\text{--}480 \text{ nm}$). (d) Upconversion luminescence intensity profile of panel b.

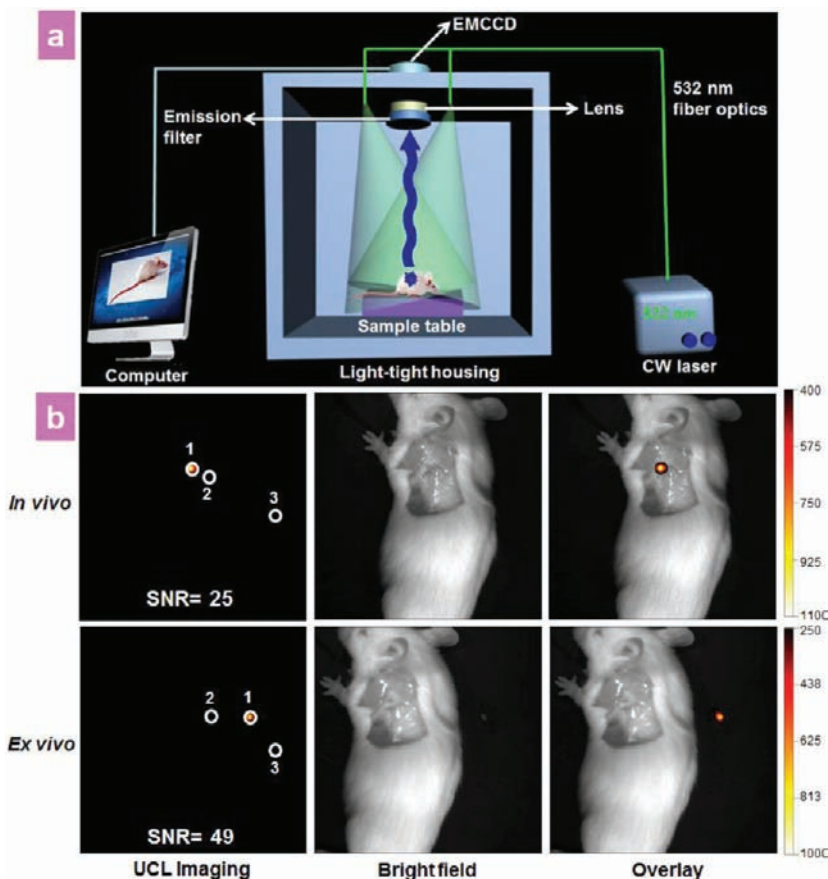


Figure 7. (a) Schematic layout of the experimental setup for the upconversion luminescence in vivo imaging system designed by our group. Two external 0–500 mW adjustable CW 532 nm lasers were used as the excitation sources, and an Andor DU897 EMCCD was used as the signal collector. (b) In vivo and ex vivo upconversion luminescence lymphatic imaging at 30 min postinjection of 20 μL of TTA-UCNP in paw. $\lambda_{\text{ex}} = 532 \text{ nm}$ (the power density of $\sim 8.5 \text{ mW cm}^{-2}$), $\lambda_{\text{em}} < 525 \text{ nm}$. Signal to noise ratio (SNR) = [(mean luminescence intensity of region 1) – (mean luminescence intensity of region 3)] / [(mean luminescence intensity of the region 2) – (mean luminescence intensity of the region 3)].

of $8.5 \times 10^{-17} \text{ cm}^2$ for the sensitizer PdOEP and high ϕ_{UCL} of 4.5% for the TTA-UCNP.

CONCLUSION

In summary, water-soluble nanoparticles showing triplet-triplet annihilation-based upconversion luminescence were successfully prepared by loading sensitizer (PdOEP) and annihilator (DPA) into silica nanoparticles. The upconversion luminescence quantum yield of the nanoparticles can be as high as 4.5% in pure water. The upconversion nanoparticles were successfully used to label living cells with very high signal-to-noise ratio and excellent photostability. In particular, such blue-emissive upconversion nanoparticles were successfully applied in lymph node imaging in vivo of living mouse with excellent signal-to-noise ratio (>25), upon low-power density excitation of CW laser (8.5 mW cm^{-2}). This study opens new perspectives for TTA-based upconversion luminescence materials in bioimaging in vivo applications.

ASSOCIATED CONTENT

Supporting Information

Absorption and UCL spectra of DPA and PdOEP in toluene; UCL spectrum and continuous kinetic scan of TTA-UCNP; UCL spectra of TTA in water, PBS, and serum; schematic layout of confocal fluorescence microscopy ($\lambda_{\text{ex}} = 405 \text{ nm}$); Z-stack confocal imaging; and UCL imaging. This material is available free of charge via the Internet at <http://pubs.acs.org>.

AUTHOR INFORMATION

Corresponding Author

fyli@fudan.edu.cn

Notes

The authors declare no competing financial interest.

ACKNOWLEDGMENTS

This work was financially supported by China National Funds for Distinguished Young Scientists from the NSFC (20825101), NSFC (91027004), SSTC (11XD1400200 and 1052 nm03400), the State Key Basic Research Program of China (2011AA03A407 and 2012CB932403), IRT0911, SLADP (B108), and the CAS/SAFEA International Partnership Program for Creative Research Teams.

REFERENCES

- (1) (a) Auzel, F. *Chem. Rev.* **2004**, *104*, 139–173. (b) Wang, F.; Liu, X. G. *Chem. Soc. Rev.* **2009**, *38*, 976–989. (c) Zhou, J.; Liu, Z.; Li, F. Y. *Chem. Soc. Rev.* **2012**, *41*, 1323–1349. (d) Haase, M.; Schäfer, H. *Angew. Chem., Int. Ed.* **2011**, *50*, 5808–5829. (e) Wang, G. F.; Peng, Q.; Li, Y. D. *Acc. Chem. Res.* **2011**, *44*, 322–332. (f) Wang, F.; Banerjee, D.; Liu, Y. S.; Chen, X. Y.; Liu, X. G. *Analyst* **2010**, *135*, 1839–1854. (g) Li, C. X.; Lin, J. J. *Mater. Chem.* **2010**, *20*, 6831–6847. (h) Feng, W.; Sun, L. D.; Zhang, Y. W.; Yan, C. H. *Coord. Chem. Rev.* **2010**, *254*, 1038–1053.
- (2) Rachford, T. N. S.; Castellano, F. N. *Coord. Chem. Rev.* **2010**, *254*, 2560–2573.
- (3) (a) Wang, X.; Zhuang, J.; Peng, Q.; Li, Y. D. *Nature* **2005**, *437*, 121–124. (b) Wang, G. F.; Peng, Q.; Li, Y. D. *J. Am. Chem. Soc.* **2009**, *131*, 14200–14201. (c) Wang, F.; Han, Y.; Lim, C. S.; Lu, Y.; Wang, J.; Xu, J.; Chen, H.; Zhang, C.; Hong, M.; Liu, X. G. *Nature* **2010**, *463*, 1061–1065. (d) Wu, S. W.; Han, G.; Milliron, D. J.; Aloni, S.; Altoe, V.; Talapin, D. V.; Cohen, B. E.; Schuck, P. J. *Proc. Natl. Acad. Sci. U.S.A.* **2009**, *106*, 10917–10921. (e) Fischer, L. H.; Harms, G. S.; Wolfbeis, O. S. *Angew. Chem., Int. Ed.* **2011**, *50*, 4546–4551. (f) Achatz, D. E.; Meier, R. J.; Fischer, L. H.; Wolfbeis, O. S. *Angew. Chem., Int. Ed.* **2011**, *50*, 260–263. (g) Chen, G. Y.; Ohulchanskyy, T. Y.; Kumar, R.; Agren, H.; Prasad, P. N. *ACS Nano* **2010**, *4*, 3163–3168. (h) Mai, H. X.; Zhang, Y. W.; Si, R.; Yan, Z. G.; Sun, L. D.; You, L. P.; Yan, C. H. *J. Am. Chem. Soc.* **2006**, *128*, 6426–6436. (i) Vetrone, F.; Naccache, R.; Mahalingam, V.; Morgan, C. G.; Capobianco, J. A. *Adv. Funct. Mater.* **2009**, *19*, 2924–2929. (j) Abel, K. A.; Boyer, J. C.; van Veggel, F. C. J. M. *J. Am. Chem. Soc.* **2009**, *131*, 14644–14645.

- (4) (a) Cahalan, M. D.; Miller, M. J.; Wei, S. H.; Parker, I. *Science* **2002**, *296*, 1869–1873. (b) Wang, B.; Wang, Y. C.; Hua, J. L.; Jiang, Y. H.; Huang, J. H.; Qian, S. X.; Tian, H. *Chem.-Eur. J.* **2011**, *17*, 2647–2655. (c) Jiang, Y. H.; Wang, Y. C.; Hua, J. L.; Tang, J.; Li, B.; Qian, S. X.; Tian, H. *Chem. Commun.* **2010**, 4689–4691.
- (5) (a) Kumar, R.; Nyk, M.; Ohulchanskyy, T. Y.; Flask, C. A.; Prasad, P. N. *Adv. Funct. Mater.* **2009**, *19*, 853–859. (b) Idris, N. M.; Li, Z. Q.; Ye, L.; Sim, E. K. W.; Mahendran, R.; Ho, P. C. L.; Zhang, Y. *Biomaterials* **2009**, *30*, 5104–5113. (c) Bogdan, N.; Vetrone, F.; Roy, R.; Capobianco, J. A. *J. Mater. Chem.* **2010**, *20*, 7543–7550. (d) Chen, F.; Bu, W. B.; Zhang, S. J.; Liu, X. H.; Liu, J. N.; Xing, H. Y.; Xiao, Q. F.; Zhou, L. P.; Peng, W. J.; Wang, L. Z.; Shi, J. L. *Adv. Funct. Mater.* **2011**, *21*, 4285–4294. (e) Xing, H. Y.; Bu, W. B.; Zhang, S. J.; Zheng, X. P.; Li, M.; Chen, F.; He, Q. J.; Zhou, L. P.; Peng, W. J.; Hua, Y. Q.; Shi, J. L. *Biomaterials* **2012**, *33*, 1079–1089. (f) Wang, C.; Chen, L.; Liu, Z. *Biomaterials* **2011**, *32*, 1110–1120. (g) Cheng, L.; Yang, K.; Li, Y. G.; Chen, J. H.; Wang, C.; Shao, M.; Lee, S. T.; Liu, Z. *Angew. Chem., Int. Ed.* **2011**, *50*, 7385–7390. (h) Ju, Q.; Tu, D.; Liu, Y. S.; Li, R. F.; Zhu, H. M.; Chen, J. C.; Chen, Z.; Huang, M. D.; Chen, X. Y. *J. Am. Chem. Soc.* **2012**, *134*, 1323–1330.
- (6) (a) Yu, M. X.; Li, F. Y.; Chen, Z. G.; Hu, H.; Zhan, C.; Yang, H.; Huang, C. H. *Anal. Chem.* **2009**, *81*, 930–935. (b) Xiong, L. Q.; Chen, Z. G.; Tian, Q. W.; Cao, T. Y.; Xu, C. J.; Li, F. Y. *Anal. Chem.* **2009**, *81*, 8687–8694. (c) Chen, Z. G.; Chen, H. L.; Hu, H.; Yu, M. X.; Li, F. Y.; Zhang, Q.; Zhou, Z. G.; Yi, T.; Huang, C. H. *J. Am. Chem. Soc.* **2008**, *130*, 3023–3029. (d) Liu, J. L.; Liu, Y.; Liu, Q.; Li, C. Y.; Sun, L. N.; Li, F. Y. *J. Am. Chem. Soc.* **2011**, *133*, 15276–15279. (e) Liu, Q.; Peng, J. J.; Li, C. Y.; Sun, L. N.; Li, F. Y. *ACS Nano* **2011**, *5*, 8040–8048. (f) Zhou, J.; Sun, Y.; Du, X. X.; Xiong, L. Q.; Hu, H.; Li, F. Y. *Biomaterials* **2010**, *31*, 3287–3285. (g) Zhou, J.; Yu, M. X.; Sun, Y.; Zhang, X. Z.; Zhu, X. J.; Wu, Z. H.; Wu, D. M.; Li, F. Y. *Biomaterials* **2011**, *32*, 1148–1156. (h) Liu, Q.; Sun, Y.; Li, C. G.; Zhou, J.; Li, C. Y.; Yang, T. S.; Zhang, X. Z.; Yi, T.; Wu, D. M.; Li, F. Y. *ACS Nano* **2011**, *5*, 3146–3157.
- (7) Liu, Q.; Sun, Y.; Yang, T. S.; Feng, W.; Li, C. G.; Li, F. Y. *J. Am. Chem. Soc.* **2011**, *133*, 17122–17125.
- (8) Zhang, Q. Q.; Qian, J.; Liang, H. J.; Somesfalean, G.; Wang, D.; Zhang, Z. G.; Andersson-Engels, S. *ACS Nano* **2011**, *5*, 3744–3757.
- (9) Li, S. F.; Zhang, M.; Peng, Y.; Zhang, Q. Y.; Zhao, M. S. *J. Rare Earths* **2010**, *28*, 237–242.
- (10) Boyer, J. C.; van Veggel, F. C. J. M. *Nanoscale* **2010**, *2*, 1417–1419.
- (11) Parker, C. A.; Hatchard, C. G.; Joyce, T. A. *Nature* **1965**, *20*, 1282–1284.
- (12) (a) Singh-Rachford, T. N.; Haeefe, A.; Ziessel, R.; Castellano, F. N. *J. Am. Chem. Soc.* **2008**, *130*, 16164–16165. (b) Islangulov, R. R.; Castellano, F. N. *Angew. Chem., Int. Ed.* **2006**, *45*, 5957–5959. (c) Islangulov, R. R.; Lott, J.; Weder, C.; Castellano, F. N. *J. Am. Chem. Soc.* **2007**, *129*, 12652–12653. (d) Singh-Rachford, T. N.; Lott, J.; Weder, C.; Castellano, F. N. *J. Am. Chem. Soc.* **2009**, *131*, 12007–12014. (e) Islangulov, R. R.; Kozlov, D. V.; Castellano, F. N. *Chem. Commun.* **2005**, 3776–3778. (f) Zhao, W.; Castellano, F. N. *J. Phys. Chem. A* **2006**, *110*, 11440–11445. (g) Singh-Rachford, T. N.; Castellano, F. N. *J. Phys. Chem. A* **2008**, *112*, 3550–3556. (h) Khnayzer, R. S.; Blumhoff, J.; Harrington, J. A.; Haeefe, A.; Deng, F.; Castellano, F. N. *Chem. Commun.* **2012**, *48*, 209–211. (i) Haeefe, A.; Blumhoff, J.; Khnayzer, R. S.; Castellano, F. N. *J. Phys. Chem. Lett.* **2012**, *3*, 299–303.
- (13) (a) Ji, S. M.; Wu, W. H.; Wu, W. T.; Zhao, J. Z. *Angew. Chem., Int. Ed.* **2011**, *50*, 8283–8286. (b) Ji, S. M.; Wu, W. H.; Wu, W. T.; Zhao, J. Z. *Angew. Chem., Int. Ed.* **2011**, *50*, 1626–1629. (c) Guo, H.

M.; Sun, H. Y.; Wu, W. T.; Liu, X.; Zhao, J. Z. *Dalton Trans.* **2011**, *40*, 7834–7841.

(14) (a) Cheng, Y. Y.; Khoury, T.; Clady, R. G. C. R.; Tayebjee, M. J. Y.; Ekins-ukes, N. J.; Crossley, M. J. *Phys. Chem. Chem. Phys.* **2010**, *12*, 66–71. (b) Monguzzi, A.; Mezyk, J.; Scotognella, F.; Tubino, R.; Meinardi, F. *Phys. Rev. B* **2008**, *78*, 195112. (c) Balushev, S.; Yakutkin, V.; Miteva, T.; Wegner, G.; Roberts, T.; Nelles, G.; Yasuda, A.; Chernov, S.; Aleshchenkov, S.; Cheprakov, A. *New J. Phys.* **2008**, *10*, 013007. (d) Du, P. W.; Eisenberg, R. *Chem. Sci.* **2010**, *1*, 502–506. (e) Yamada, H.; Kuzuhara, D.; Ohkubo, K.; Takahashi, T.; Okujima, T.; Uno, H.; Ono, N.; Fukuzumi, S. *J. Mater. Chem.* **2010**, *20*, 3011–3024.

(15) (a) Tanaka, K.; Inafuku, K.; Chujo, Y. *Chem. Commun.* **2010**, 4378–4380. (b) Wohnhaas, C.; Turshatov, A.; Mailnder, V.; Lorenz, S.; Balushev, S.; Miteva, T.; Landfester, K. *Macromol. Biosci.* **2011**, *11*, 772–778. (c) Turshatov, A.; Busko, D.; Balushev, S.; Miteva, T.; Landfester, K. *New J. Phys.* **2011**, *10*, 083035.

(16) Zanarini, S.; Rampazzo, E.; Bonacchi, S.; Juris, R.; Marcaccio, M.; Montalti, M.; Paolucci, F.; Prodi, L. *J. Am. Chem. Soc.* **2009**, *131*, 14208–14209.

(17) (a) Filipescu, N.; Mushrush, G. W.; Hurt, C. R.; Mcavoy, N. *Nature* **1966**, *211*, 960–961. (b) Monguzzi, A.; Frigoli, M.; Larpent, C.; Tubino, R.; Meinardi, F. *Adv. Funct. Mater.* **2012**, *22*, 139–143.